MOLECULAR AND CELLULAR BIOLOGY, Nov. 2004, p. 9414–9423 Vol. 24, No. 21
0270-7306/04/$08.00+0 DOI: 10.1128/MCB.24.21.9414–9423.2004

Essential Role for Mitochondrial Thioredoxin Reductase in Hematopoiesis, Heart Development, and Heart Function

Marcus Conrad,[1]†* Cemile Jakupoglu,[1]† Stéphanie G. Moreno,[1] Stefanie Lippl,[1] Ana Banjac,[1] Manuela Schneider,[2] Heike Beck,[1] Antonis K. Hatzopoulos,[1] Ursula Just,[1] Fred Sinowatz,[3] Wolfgang Schmahl,[4] Kenneth R. Chien,[5] Wolfgang Wurst,[6] Georg W. Bornkamm,[1]† and Markus Brielmeier[2]†

Institute of Clinical Molecular Biology and Tumour Genetics, GSF Research Centre for Environment and Health,[1] and Department of Veterinary Anatomy II[3] and Institute of Veterinary Pathology,[4] Ludwig-Maximilian University of Munich, Munich, and Department of Comparative Medicine[2] and Institute of Developmental Genetics,[6] GSF Research Centre for Environment and Health, Neuherberg, Germany, and Institute of Molecular Medicine, University of California at San Diego School of Medicine, La Jolla, California[5]

Received 18 February 2004/Returned for modification 21 April 2004/Accepted 22 July 2004

Oxygen radicals regulate many physiological processes, such as signaling, proliferation, and apoptosis, and thus play a pivotal role in pathophysiology and disease development. There are at least two thioredoxin reductase/thioredoxin/peroxiredoxin systems participating in the cellular defense against oxygen radicals. At present, relatively little is known about the contribution of individual enzymes to the redox metabolism in different cell types. To begin to address this question, we generated and characterized mice lacking functional mitochondrial thioredoxin reductase (*TrxR2*). Ubiquitous Cre-mediated inactivation of *TrxR2* is associated with embryonic death at embryonic day 13. *TrxR2*$^{-/-}$ embryos are smaller and severely anemic and show increased apoptosis in the liver. The size of hematopoietic colonies cultured ex vivo is dramatically reduced. *TrxR2*-deficient embryonic fibroblasts are highly sensitive to endogenous oxygen radicals when glutathione synthesis is inhibited. Besides the defect in hematopoiesis, the ventricular heart wall of *TrxR2*$^{-/-}$ embryos is thinned and proliferation of cardiomyocytes is decreased. Cardiac tissue-restricted ablation of *TrxR2* results in fatal dilated cardiomyopathy, a condition reminiscent of that in Keshan disease and Friedreich's ataxia. We conclude that TrxR2 plays a pivotal role in both hematopoiesis and heart function.

Reactive oxygen species (ROS)—generated mainly as a by-product of the respiratory chain or by oxidases—are implicated in the pathogenesis and pathophysiology of a variety of human diseases such as cancer, cardiovascular, and degenerative disorders. A variety of cellular antioxidant systems control the balance of free intra- and extracellular oxygen radicals. Previous efforts have addressed the physiological role of superoxide dismutases, catalases, and glutathione (GSH) peroxidases in vivo, but the role of the thioredoxin/thioredoxin reductase/peroxiredoxin system in ROS removal has only recently attracted attention.

Thioredoxins are small redox-active proteins with an essential function in DNA metabolism and repair, transcription, and cell-cell communication (1). Acting through peroxiredoxins, they also efficiently protect cells from oxidative damage (27). Cytosolic (Trx1) and mitochondrial (Trx2) thioredoxins are required for proliferation and protection from apoptosis during early embryogenesis (26). Moreover, in chicken B cells, Trx2 is critically involved in the regulation of mitochondrion-dependent apoptosis (37). More recently, heart-specific overexpression of dominant-negative *Trx1* was shown to be associated with increased oxidative stress and cardiac hypertrophy in mice (39).

Trx activities are governed by thioredoxin reductases (TrxRs) that, in turn, use NADPH/H$^+$ as the reducing agent (23). TrxRs are members of the pyridine nucleotide-disulfide oxidoreductase family, form homodimers, and possess two interacting redox-active centers. The C-terminal redox center contains a catalytically important selenocysteine (SeCys) (9, 17, 41). In mammals, three TrxRs are known—one cytosolic (*TrxR1*) (8), one mitochondrial (*TrxR2*) (7), and one testis-specific GSH-TrxR (33)— each encoded by individual genes. In contrast to their well-studied biochemical properties, little is known about the individual contribution of the different TrxRs in living organisms or about possible redundancies among the different redox systems. To dissect the complex network of redox metabolism in vivo, we have established mice deficient for mitochondrial *TrxR2*. To overcome possible embryonic lethality, as observed in *Trx1*- and *Trx2*-null mice, and to investigate TrxR2 function in specific organs and at defined time points, we used a conditional ablation strategy. Ubiquitous deletion of *TrxR2* results in embryonic lethality at embryonic day 13 (E13). *TrxR2*$^{-/-}$ embryos are severely anemic and exhibit a marked thinning of the ventricular heart wall. To further dissect the contribution of the two major defects in the overall phenotype, we generated mice with cardiac cell-specific inactivation of the *TrxR2* gene. These mice developed fatal dilated cardiomyopathy and died shortly after birth. Analysis of fibroblasts isolated from *TrxR2*$^{-/-}$ embryos revealed a critical role of TrxR2 in the

* Corresponding author. Mailing address: Institute of Clinical Molecular Biology and Tumour Genetics, GSF Research Centre for Environment and Health, Marchioninistr. 25, D-81377 Munich, Germany. Phone: 49-89-7099525. Fax: 49-89-7099500. E-mail: marcus.conrad@gsf.de.

† M.C., C.J., G.W.B., and M.B. contributed equally to this study.

removal of toxic ROS species and the maintenance of mitochondrial integrity.

MATERIALS AND METHODS

Gene targeting, mouse breeding and genotyping. Mouse expressed sequence tag clone IMAGp998N131993 (RZPD, Berlin, Germany), covering exons 10 to 18 of *TrxR2*, was used to screen a *129/SV* mouse lambda-phage library (Stratagene, Inc., La Jolla, Calif.). Five clones were isolated and cloned into pBluescript SK(+) (Stratagene). The insert of one clone containing the 3′ region of the *TrxR2* gene was sequenced and used for the generation of the targeting constructs. In brief, a NheI/XmaI fragment representing the 5′ arm for homologous recombination was subcloned in pBluescript SK(+), and a loxP element, including an EcoRI site, was inserted in the unique FseI site. The 3′ arm was inserted as an XmaI/XmaI fragment in pPNT4, a vector containing an frt-flanked *neomycin phosphotransferase* (*neo*) gene and one loxP site (4). The targeting construct pPNT11 was completed by inserting the 5′ arm including the second loxP site. The conditional *lacZ* knockin construct is comprised of the same homologous arms but contains additional elements as depicted in Fig. 1E. Gene targeting of both constructs in E14 embryonic stem (ES) cells was carried out as described previously (14). ES cell clones with successful homologous recombination arose at a frequency of 5 to 8% when tested with both external probes pMC67 and pMC68. Additional integration sites were excluded by Southern blot analysis with a *neo* gene probe. Flp-mediated removal of the *neo* gene by transient overexpression of Flp recombinase in targeted ES cell clones occurred at a frequency of 6% (29). Backcross of chimeric animals to C57BL/6 mice, produced upon microinjection of ES cell clones into C57BL/6 blastocysts, gave rise to germ line transmission of the loxP flanked (floxed) *TrxR2* allele (11). These mice were crossed to congenic C57BL/6 Cre deleter mice, resulting in deletion of the floxed allele (31). Mice with either the floxed or the deleted *TrxR2* allele were backcrossed on a C57BL/6 background. To facilitate genotyping of mice, primer pairs were designed for detection of wild-type (WT), floxed, or deleted alleles (TrxR2flox1/2, CAGGTCACTAGGCTGTAGAGTTTGC/ATGTCCCAGTGTACTTATGATGAATC; TrxR2Del1/2, TGCTTCCAGGCCCAGTGCTCTGACTGG/CAGGCTCCTGTAGGCCCATTAAGGTGC). The Cre-specific primer pair was as follows: GATGCAACGAGTGATGAGGTTCGC/ACCCTGATCCTGGCAATTTCGGC (CreA/B).

TrxR2 was deleted in cardiomyocytes by using the *MLC2a-Cre* transgenic mouse line (38). $TrxR2^{+/-}$ mice were first crossed with *MLC2a-Cre* mice and then $TrxR2^{+/-,Tg[MLC2a\text{-}Cre]}$ and $TrxR2^{fl/fl}$ mice were mated to obtain $TrxR2^{fl/-,Tg[MLC2a\text{-}Cre]}$ mice.

Mice were kept under standard conditions with food and water ad libitum (Altromin GmbH, Lage, Germany). All animal experiments were performed in compliance with the German animal welfare law and have been approved by the institutional committee on animal experimentation and the government of Upper Bavaria.

RNA isolation and semiquantitative reverse transcription-PCR (RT-PCR). Total RNA was isolated from homogenized embryonic tissue by using peqGOLDTriFast (peqLab, Erlangen, Germany). DNase-treated total RNA (DNase I, RNase I free, catalog no. 776785; Roche, Mannheim, Germany) was reverse transcribed by using a reverse transcription system (Promega Corp., Madison, Wis.). Primer pairs specific for *Aldolase* (Aldolase1/2, AGCTGTCTGACATCGCTCACCG/CACATACTGGCAGCGCTTCAAG) and *TrxR2* (TrxR2E6/10, CAGCTTTGTGGATGAGCACACAGTTCG/GATCCTCCCAAGTGACCTGCAGCTGG; and TrxR2E15/18, TTCACGGTGGCGGATAGGGATGC/TGCCCAGGCCATCATCATCTGACG) were used to detect the transcripts.

In situ end labeling (ISEL). Detection of apoptotic cells was performed with the ApopTag kit (S7100; Serologicals Corp., Norcross, Ga.) on PFA-fixed (4% [wt/vol] paraformaldehyde [PFA] in phosphate-buffered saline), paraffin-embedded sections according to the manufacturer's instructions. Digoxigenin-deoxynucleoside triphosphate-labeled cells were incubated with an anti-digoxigenin peroxidase conjugate and visualized with 3,3′-diaminobenzidine (DAB, SK-4100; Vector Laboratories, Inc., Burlingame, Calif.).

Immunohistochemistry. (i) LacZ staining. Upon standard pretreatment and blocking with M.O.M. blocking reagent (M.O.M Immunodetection Kit, PK-2200; Vector Laboratories), cryosections were incubated overnight with an anti-β-galactosidase monoclonal antibody (1:50; MAB1802; Chemicon International, Inc., Temecula, Calif.). Visualization of avidin-biotin complexes was performed with 3-amino-9-ethylcarbazole (SK-4200; Vector Laboratories).

(ii) PCNA staining. PFA-fixed paraffin-embedded sections were incubated for 1 h at 37°C with anti-PCNA monoclonal antibody (1:200; PC10; Dako, Glostrup, Denmark) and visualized with DAB.

(iii) Double antibody-apoptosis labeling. Cryosections were incubated overnight at 4°C with a rat anti-mouse CD45 antibody (1:20; catalog no. 550539; BD Pharmingen, San Jose, Calif.). In the case of rat anti-K8 or -K18 antibodies, initial incubation was performed for 90 min at 37°C (1:10; Troma1 and Troma2 [kindly provided by Solange Magre, CNRS/Université Pierre et Marie Curie, Paris, France, and Rolf Kemler, Max Planck Institute, Freiburg, Germany]). Sections were subsequently incubated with a secondary biotinylated antibody for 1 h at room temperature. After avidin-biotin complex reaction was performed (ABC alkaline phosphatase staining kit, AK-5000; Vector Laboratories), bound antibodies were visualized with a substrate for alkaline phosphatase (Vector Blue, SK-5300; Vector Laboratories). Sections were washed and postfixed in cold ethanol-acetic acid (2:1) at −20°C, the endogenous peroxidase activity was blocked with 3% (vol/vol) H_2O_2, and the sections were subjected to the standard ISEL procedure.

Electron microscopy. Hearts were isolated and immediately fixed in 2.5% glutaraldehyde–2% PFA in 0.1 M sodium cacodylate buffer (pH 7.2) for 24 h, rinsed three times in the same buffer, and postfixed in 1% osmium tetroxide–1.5% potassium ferrocyanide in potassium cacodylate buffer for 2 h. Samples were washed three times, dehydrated, and embedded in Propylenoxyd and Polyembed 812 (Plano, Wetzlar, Germany). Ultrathin sections (60 nm) were stained with uranyl acetate and lead acetate and then examined on a Zeiss 902 electron microscope at 80 kV.

BrdU incorporation and detection. 5-Bromodeoxyuridine (BrdU; catalog no. 100171; ICN Biomedicals, Aurora, Ohio) was injected intraperitoneally in pregnant mice at E13.0 at a dose of 100 mg/kg of body weight. After 2 h, isolated embryos were fixed in PFA and embedded in paraffin. Incorporated BrdU was visualized by immunohistochemistry with an anti-BrdU monoclonal antibody (catalog no. 1170376; Roche Diagnostics Corp.) and a secondary biotinylated antibody (ABC peroxidase staining).

Mouse embryonic fibroblast (MEF) culture. Embryos were isolated from pregnant mice at E12.5, the body trunk was dissected away from other structures and then treated with trypsin, treated with DNase, minced with a syringe, and cultivated under standard conditions in Dulbecco modified Eagle medium (Invitrogen GmbH, Karlsruhe, Germany) with 10% fetal calf serum (FCS), glutamine, and penicillin-streptomycin. Buthionine sulfoximine (BSO; Sigma-Aldrich, Taufkirchen, Germany) was used at a 50 μM final concentration.

Staining of MEFs. Cell nuclei were stained with 1 μM Hoechst 33342 (Sigma-Aldrich), and the mitochondria were stained with 0.5 μM MitoTracker Green FM (Molecular Probes, Inc., Oreg.). RedoxSensor Red CC-1 was used according to the manufacturer's protocol (2) (Molecular Probes). Stained cells were assessed with a Zeiss Axiovert 200 M microscope (Carl Zeiss, Jena, Germany) and Openlab software (version 3.0; Improvision, Coventry, United Kingdom).

CFU assays. CFU assays were performed as described previously (30). In brief, livers from E12.5 embryos were prepared, minced with a syringe in Iscove modified Dulbecco medium (including 20% FCS), centrifuged, and resuspended for hemolysis in 1 volume of medium without FCS and 1 volume of 2× hemolysis buffer (1.5 M NH_4Cl, 0.1 M $KHCO_3$, and 1 mM EDTA in 500 ml [pH 7.4] with KOH). The hemolysis step was repeated twice. Cells were plated at equal cell numbers on 35-mm dishes containing methylcellulose, 10% bovine serum albumin (catalog no. 652237; Roche), 20% FCS (pretested), 1% penicillin-streptomycin, 1% glutamine, 50 μM β-mercaptoethanol, and cytokines (100 U of mouse interleukin-3 [IL-3] conditioned medium, 2 U of erythropoietin, 10 ng of stem cell factor, 10 ng of FLIT ligand, 10 ng of thrombopoietin, 10 ng of granulocyte-macrophage colony-stimulating factor, and 10 ng of IL-6/ml). After 1 week of incubation, colonies with >50 cells were counted and subdivided into granulocytes, macrophages, mixed colonies (more than three different cell types), granulocytes and macrophages, and burst-forming units that were additionally visualized by benzidine staining (0.1 volume of benzidine, 0.1 volume of H_2O_2, and 0.5 volume of H_2O).

RESULTS

Generation of *TrxR2*-deficient and *lacZ* knockin reporter mice and embryonic expression pattern of TrxR2. The *TrxR2* gene is composed of 18 exons spanning a region of 57 kb (22). The last four exons harboring the C-terminal catalytic center were flanked by two loxP sites (Fig. 1A). The SeCys codon UGA is encoded by exon 17. The selenocysteine insertion sequence (SECIS) element, essential for cotranslational SeCys incorporation at the UGA codon, and the transcription termi-

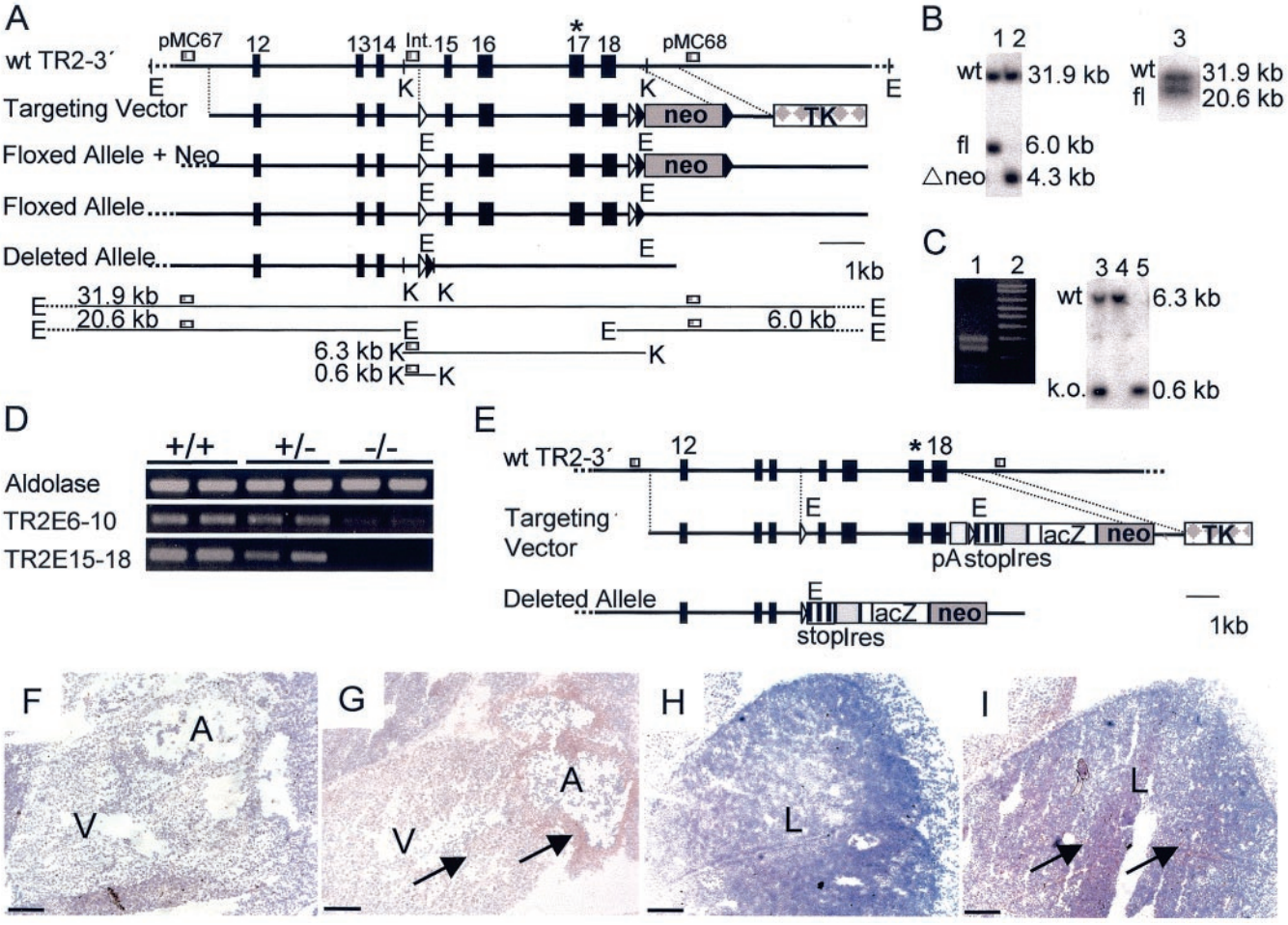

FIG. 1. Gene targeting and expression pattern of *TrxR2* in mice. (A) Strategy for conditional disruption of the *TrxR2* gene. The 3′ region of the *TrxR2* gene including exons 12 to 18 is shown in the upper line. The SeCys codon UGA is marked with an asterisk. For conditional gene targeting, exons 15 to 18 were flanked with loxP sites (open triangles). Homologous recombination, subsequent Flp-mediated removal of the frt (black triangles)-flanked *neomycin phosphotransferase* gene (*neo*), and Cre-mediated deletion of the C-terminally located redox-center are outlined below. Underneath, the expected DNA fragments from characteristic restriction digests (E, EcoRI; K, KpnI) detected with the corresponding 5′ (pMC67), 3′ (pMC68) and internal (int.) probes (striped rectangles) are schematically depicted. In the targeting vector the *thymidine kinase* gene (*TK*) is placed downstream from the 3′ arm for negative selection. (B) Homologous recombination in ES cell clones was confirmed by Southern blotting of EcoRI-digested DNA hybridized with 3′ (lanes 1 and 2) and 5′ (lane 3) external probes and after removal of the *neo* gene (lane 2). (C) Germ line transmission of the modified *TrxR2* allele was verified by PCR genotyping of tail DNA (lanes 1 and 2). The floxed *TrxR2* allele gives rise to a 40-bp-longer product than the WT allele (lane 1; lane 2, 100-bp ladder). Southern blotting of KpnI-digested DNA, isolated from E12.5 embryos of $TrxR2^{+/-}$ intercrosses, was hybridized with the internal probe (lanes 3 to 5) revealing heterozygous (lane 3), WT (lane 4), and KO (lane 5) embryos. (D) Semiquantitative RT-PCR analyses of mRNA obtained from E12.5 embryos of $TrxR2^{+/-}$ intercrosses. (E) Additional gene targeting strategy to study the *TrxR2* expression pattern with β-galactosidase as a reporter gene. $TrxR2^{+/-[lacZk.i.]}$ mice were generated and identified by Southern blotting as described in panels B and C. (F to I) Immunohistochemistry of $TrxR2^{+/+}$ (F and H) and $TrxR2^{+/-[lacZ\ k.i.]}$ (G and I) embryos stained with an anti-lacZ antibody (brown color; arrows) revealed strong expression in the atrium (A) and ventricle (V) of the heart (F and G) and lower expression in the liver (H and I). Cryosections were counterstained with hematoxylin. Scale bars (F to I), 100 μm.

nation signal are both encoded by exon 18. After homologous recombination of the targeting construct in ES cells (Fig. 1A and B), Flp-mediated removal of the frt-flanked *neomycin phosphotransferase* gene (*neo*) in ES cells results in a *TrxR2* allele with two loxP and one frt inserted sites. Cre-mediated excision of the loxP-flanked exons 15 to 18 in mice leads to removal of the C-terminally located enzymatic domain of TrxR2 (Fig. 1C). $TrxR2^{+/-}$ mice, obtained after breeding with Cre deleter mice, are viable and fertile, show no obvious phenotype, and have a normal life span compared to WT littermates. Since no specific antibody for the detection of TrxR2 was available, semiquantitative RT-PCR with embryonic mRNA was used to verify the knockout (KO) of the targeted region (Fig. 1D). Two primer pairs, one covering the central region (TrxR2E6-10) and one covering the deleted region (TrxR2E15-18) of the *TrxR2* gene, were used to study mRNA levels in embryos. Aldolase served as a control. The absence of the last four exons in $TrxR2^{-/-}$ embryos was confirmed with primer pair TrxR2E15-18. Reduction of mRNA levels was noticeable in $TrxR2^{+/-}$ embryos compared to WT siblings. Faint RT-PCR products were observed in $TrxR2^{-/-}$ embryos with primer pair TrxR2E6-10, indicating very low levels of truncated TrxR2 message.

To study the *TrxR2* expression pattern, we designed a con-

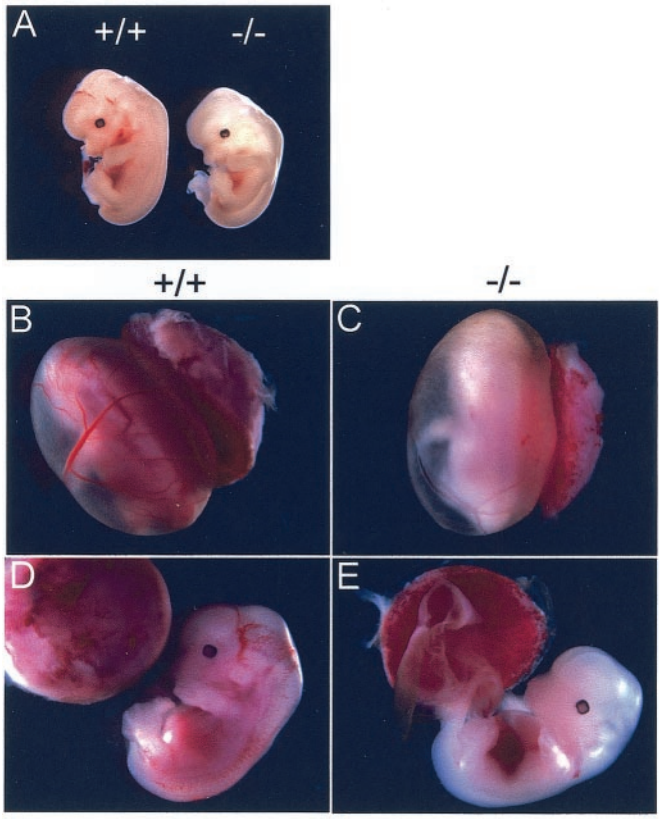

FIG. 2. Anemic appearance of *TrxR2*$^{-/-}$ embryos. (A) *TrxR2*$^{-/-}$ embryos (right) are anemic and smaller than WT littermates (left) but do not display any gross developmental abnormalities. (B to E) The blood vessels of freshly prepared *TrxR2*$^{-/-}$ embryos (E13.5) (C and E) were less supplied with blood than *TrxR2*$^{+/+}$ littermates (B and D) as best seen in the yolk sac (B and C) and developing brain (D and E). Placenta formation was not affected (B and E), as also confirmed by histological examination (data not shown).

ditional *lacZ* knockin approach into the *TrxR2* locus (Fig. 1E). A translational and transcriptional stop/internal ribosomal entry site–β-galactosidase(*lacZ*) cassette was placed in the 3′-nontranscribed region of the *TrxR2* gene. This brings LacZ under the control of the endogenous *TrxR2* promoter upon Cre-mediated removal of exons 15 to 18, including the transcriptional stop signal (derived from the mouse *phosphoglycerine kinase* gene). Immunohistochemistry of *TrxR2*$^{+/-(\text{lacZ-k.i.})}$ embryos with an anti-lacZ antibody revealed strong expression in the embryonic heart, especially in the myocardium and atrial walls, and to a lower extent in the embryonic liver (Fig. 1F to I). These findings are consistent with mRNA expression data obtained from adult tissues (21).

Embryonic lethality caused by *TrxR2* deficiency. Intercross of *TrxR2*$^{+/-}$ mice did not yield *TrxR2*$^{-/-}$ offspring (of 137 viable offspring, 33.6% were genotypically WT and 66.4% hemizygous). Genotyping of littermates at different days of gestation revealed that *TrxR2*$^{-/-}$ embryos died between E12.5 and E13.5. *TrxR2*$^{-/-}$ embryos were reduced in size and had an anemic appearance (Fig. 2A). The blood vessels of the yolk sac and the embryo proper were markedly less supplied with blood (Fig. 2B to E), and the bloodstream velocity was slower in living *TrxR2*$^{-/-}$ embryos at E13.0 (data not shown). The anemic appearance of the *TrxR2*$^{-/-}$ embryos and the comparable high expression of *TrxR2* in embryonic heart and liver suggested a crucial role of TrxR2 in the respective organs.

TrxR2 is required for proper heart development. Histological examination of *TrxR2*$^{-/-}$ embryos at E13.0 revealed dysplasia of cardiac tissue. The ventricular myocardium, the ventricular septum, and the trabeculae were thinner compared to WT siblings (Fig. 3A and B). No abnormalities of the valves and outflow tract were noticeable in *TrxR2*$^{-/-}$ hearts. To investigate whether reduced proliferation or increased cell death gave rise to the observed phenotype, we performed BrdU incorporation studies, as well as PCNA and ISEL staining. BrdU incorporation and PCNA staining revealed decreased proliferation in the myocardium of *TrxR2*$^{-/-}$ embryos (Fig. 3D and F). In contrast to *TrxR2*$^{-/-}$ mice (Fig. 3F), myocardial PCNA staining in *TrxR2*$^{+/+}$ littermates was more pronounced and predominantly nuclear, indicating that most cells were proliferating (Fig. 3E). No differences in the proliferation of the endocardial cushions and, unexpectedly, no increase in apoptosis throughout the heart were observed (data not shown).

We compared expression levels between WT and *TrxR2*$^{-/-}$ embryos for a number of genes important for cardiovascular development and function (including *erbB2*, *erbB4*, *erbB3*, *heregulin*, *GATA-4*, *GATA-6*, *Ang1*, *tie-2*, *VEGF*, *VEGFR2*, *ephrin-B2*, *Eph-B4*, *EGFR*, *TGF*β, *TGF*β*RII*, *ecNOS*, and *iNOS*), but we did not detect any differences (data not shown). Similarly, immunofluorescence analysis with antibodies against CD31, CD34, VEGFR2, laminin γ, collagen IV, erbB3, vWF, and VE-cadherin did not reveal any abnormal patterns in *TrxR2*$^{-/-}$ embryos (data not shown). Moreover, we did not observe any defects in vessel formation of placenta and yolk sacs of *TrxR2*$^{-/-}$ embryos (data not shown). We conclude that reduced proliferation, rather than loss, of cardiomyocytes is the cause of the thinning of the ventricular myocard in *TrxR2*$^{-/-}$ embryos.

TrxR2 is required for fetal blood cell formation. We examined whether the anemic phenotype in *TrxR2*$^{-/-}$ embryos is due to reduced heart function or whether it is caused by perturbed hematopoiesis in the liver, the main site of fetal hematopoiesis after E11 (6). Noticeable was the pleiomorphic and spongiform appearance of liver tissue in *TrxR2*$^{-/-}$ embryos, suggesting perturbed proliferation and/or increased apoptosis of hepatocytes and/or hematopoietic cells (Fig. 3G and H). BrdU and PCNA staining of embryonic liver sections did not reveal any major differences (data not shown), whereas ISEL staining showed augmented apoptosis in the liver of *TrxR2*$^{-/-}$ embryos (Fig. 3I and K). Double staining, including ISEL, blood cell marker CD45, and hepatocyte markers keratins 8 and 18, revealed that mainly blood cells were affected by the loss of TrxR2 (Fig. 3L to N). CFU assays with liver cells isolated from E12.5 embryos were carried out to investigate whether hematopoietic differentiation is perturbed. In CFU assays, the composition of blood cell colonies was unaltered (Fig. 4A). However, *TrxR2*$^{-/-}$ colonies were markedly smaller (Fig. 4B to E), indicating that reduced blood cell formation is the cause of the severe anemic phenotype of *TrxR2*$^{-/-}$ embryos.

Increased oxygen radical formation in TrxR2-deficient cells. The mitochondrial TrxR2/Trx2/peroxiredoxin-3 system is sim-

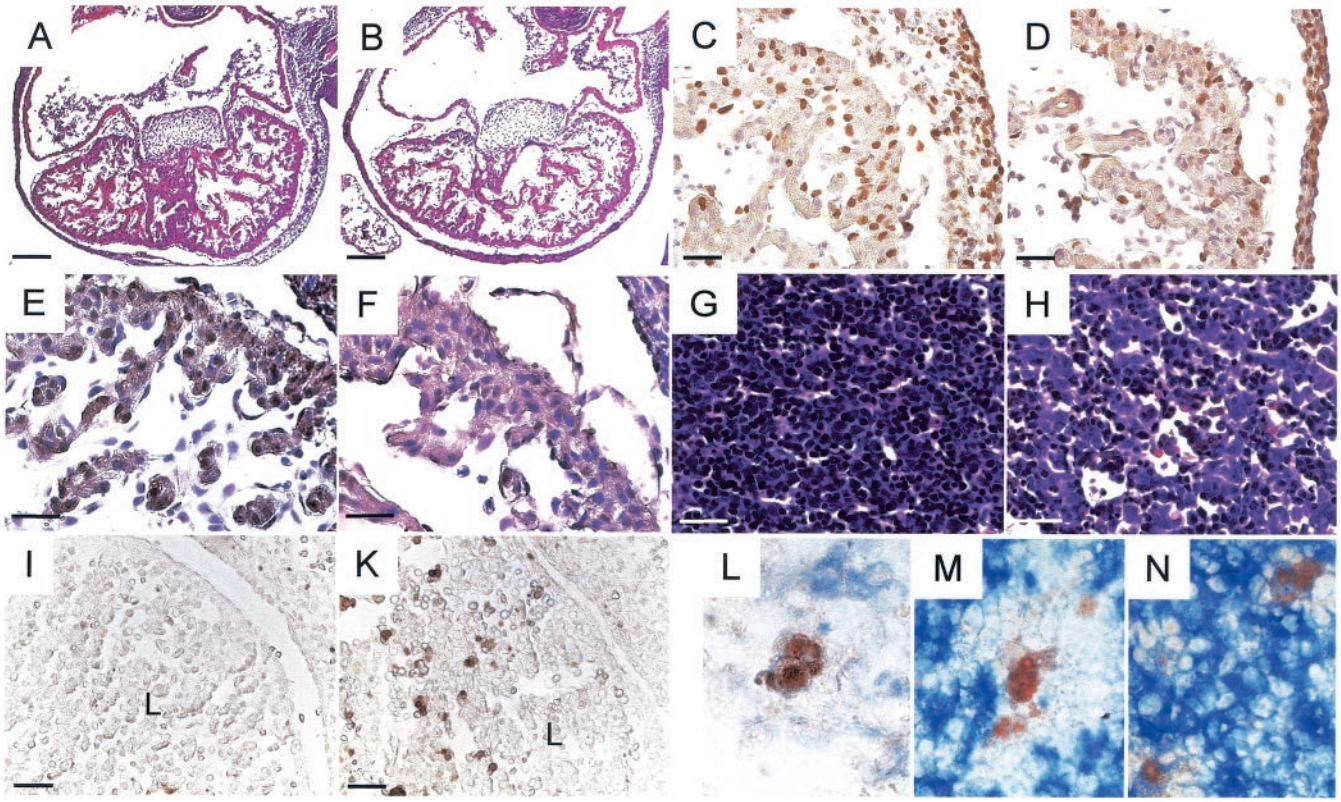

FIG. 3. Histological examination of *TrxR2*-deficient embryos. (A and B) H&E staining of transversal sections through the heart region of $TrxR2^{+/+}$ (A) and $TrxR2^{-/-}$ (B) embryos at E13.0. All basic structures of the heart are formed, but the ventricular chamber walls are thinned and the trabeculae are less prominent. The endocardial cushions and valves are not affected. BrdU incorporation (C and D) and nuclear PCNA staining (E and F) revealed reduced proliferation of myocardial cells in $TrxR2^{-/-}$ (D and F) versus $TrxR2^{+/+}$ (C and E) embryos. Hematoxylin and eosin (G and H) and ISEL staining (I and K) of liver sections revealed pleiomorphic, spongiform-like structures (H) and increased apoptosis (K) in $TrxR2^{-/-}$ embryos. ISEL-(brown) and antibody (blue)-double staining of $TrxR2^{-/-}$ liver sections revealed that part of the apoptotic cells (brown) are of hematopoietic origin (CD45-positive, L), whereas the majority of nonhematopoietic keratin 8 (m)-, and keratin 18-positive cells (N) were negative for ISEL staining. Scale bars: A and B, 100 μm; C, D, I, and K, 25 μm; E to H, 20 μm.

ilar to the cytosolic TrxR1/Trx1/peroxiredoxin-1 system (25) and is thought to be involved in the elimination of oxygen radicals generated as a by-product of oxidative phosphorylation in the respiratory chain (Fig. 4G) (15). To examine whether removal of ROS and consequently proliferation and/or apoptosis are affected in $TrxR2^{-/-}$ cells, MEFs were used as a cellular model system. Proliferation of $TrxR2^{-/-}$ MEFs was significantly slower compared to WT counterparts (Fig. 4F). Embryonic fibroblasts were stained with the RedoxSensor Red CC-1 dye for intracellular ROS accumulation. RedoxSensor Red CC-1 stains intracellular ROS and, depending on the level of ROS, it localizes to different cellular compartments (2, 36). No major difference was observed in WT versus KO MEFs, indicating that other antioxidant systems substitute for the missing TrxR2 function (data not shown). However, when the de novo synthesis of GSH was inhibited with 50 μM BSO (Fig. 4G), a competitive inhibitor of the γ-glutamyl-cysteinyl-synthetase that catalyzes the rate-limiting

FIG. 4. Hematopoietic colony formation (A to E), fibroblast proliferation (F) and removal of ROS (G to L) are severely affected in $TrxR2^{-/-}$ cells. (A to E) CFU assays were performed with isolated liver cells from E12.5 embryos. The liver cells were cultivated for 1 week. Colonies were classified as macrophages (group 1); burst-forming units (group 2); mixed colonies composed of macrophages, granulocytes, and burst-forming units (group 3); granulocytes and macrophages (group 4); and pure granulocyte colonies (group 5). (A) Differentiation into the different colony types was not altered in $TrxR2^{+/-}$ and $TrxR2^{-/-}$ cells. (B to E) The size of individual $TrxR2^{-/-}$ colonies (C and E) was, however, dramatically reduced compared to WT controls (B and D). (F) Decreased proliferation of MEFs of $TrxR2^{-/-}$ compared to $TrxR2^{+/+}$ mice. (H) When GSH synthesis was inhibited in MEFs by 50 μM BSO, cell death was rapidly induced in $TrxR2^{-/-}$ but not in $TrxR2^{+/+}$ cells. (G) The main cellular defense systems against ROS that may compensate for the loss of the *TrxR2* are schematically depicted. (I to L) Triple staining with Hoechst 33342 (blue nuclear staining), MitoTracker Green FM (green mitochondrial staining), and RedoxSensor Red CC-1 (red) after 48 h of BSO treatment revealed predominant lysosomal localization of the RedoxSensor Red CC-1 in WT cells (I) and mitochondrial localization in $TrxR2^{-/-}$ cells (K). (L) The distribution of the dyes in the different cellular compartments is quantified. (M) NAC treatment (5 mM) rescued $TrxR2^{-/-}$ MEFs from BSO-induced apoptosis. A strongly increasing number of detaching and dying cells was apparent only in KO cells (days 3 and 5) without NAC treatment. Photographs were taken at days 1, 3, and 5 after BSO and NAC treatment. (H) Quantification of the results.

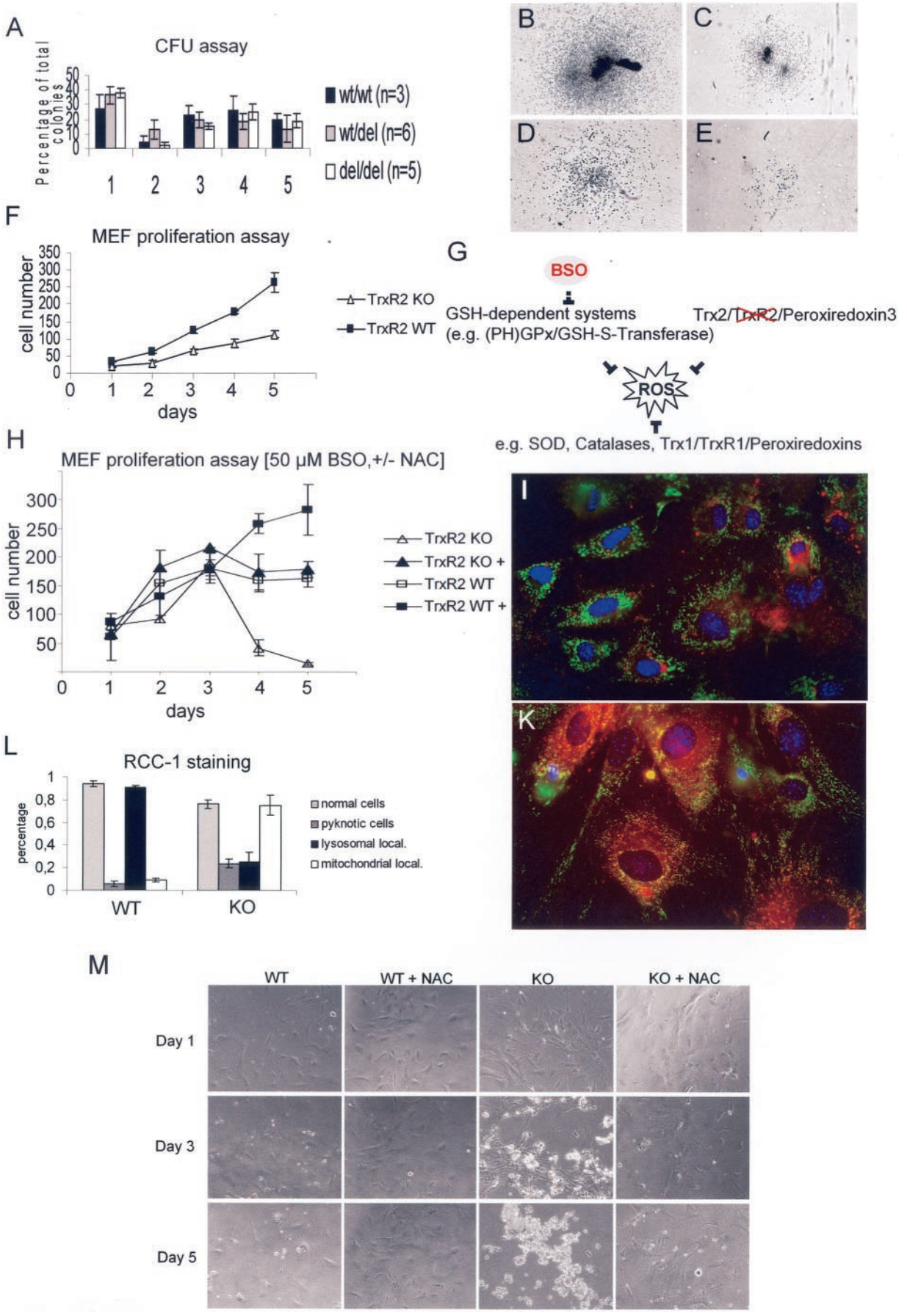
A
CFU assay
Percentage of total colonies
wt/wt (n=3)
wt/del (n=6)
del/del (n=5)
B
C
D
E
F
MEF proliferation assay
cell number
days
TrxR2 KO
TrxR2 WT
G
BSO
GSH-dependent systems
(e.g. (PH)GPx/GSH-S-Transferase)
Trx2/TrxR2/Peroxiredoxin3
ROS
e.g. SOD, Catalases, Trx1/TrxR1/Peroxiredoxins
H
MEF proliferation assay [50 µM BSO,+/- NAC]
cell number
days
TrxR2 KO
TrxR2 KO +
TrxR2 WT
TrxR2 WT +
I
K
L
RCC-1 staining
percentage
normal cells
pyknotic cells
lysosomal local.
mitochondrial local.
WT
KO
M
WT
WT + NAC
KO
KO + NAC
Day 1
Day 3
Day 5

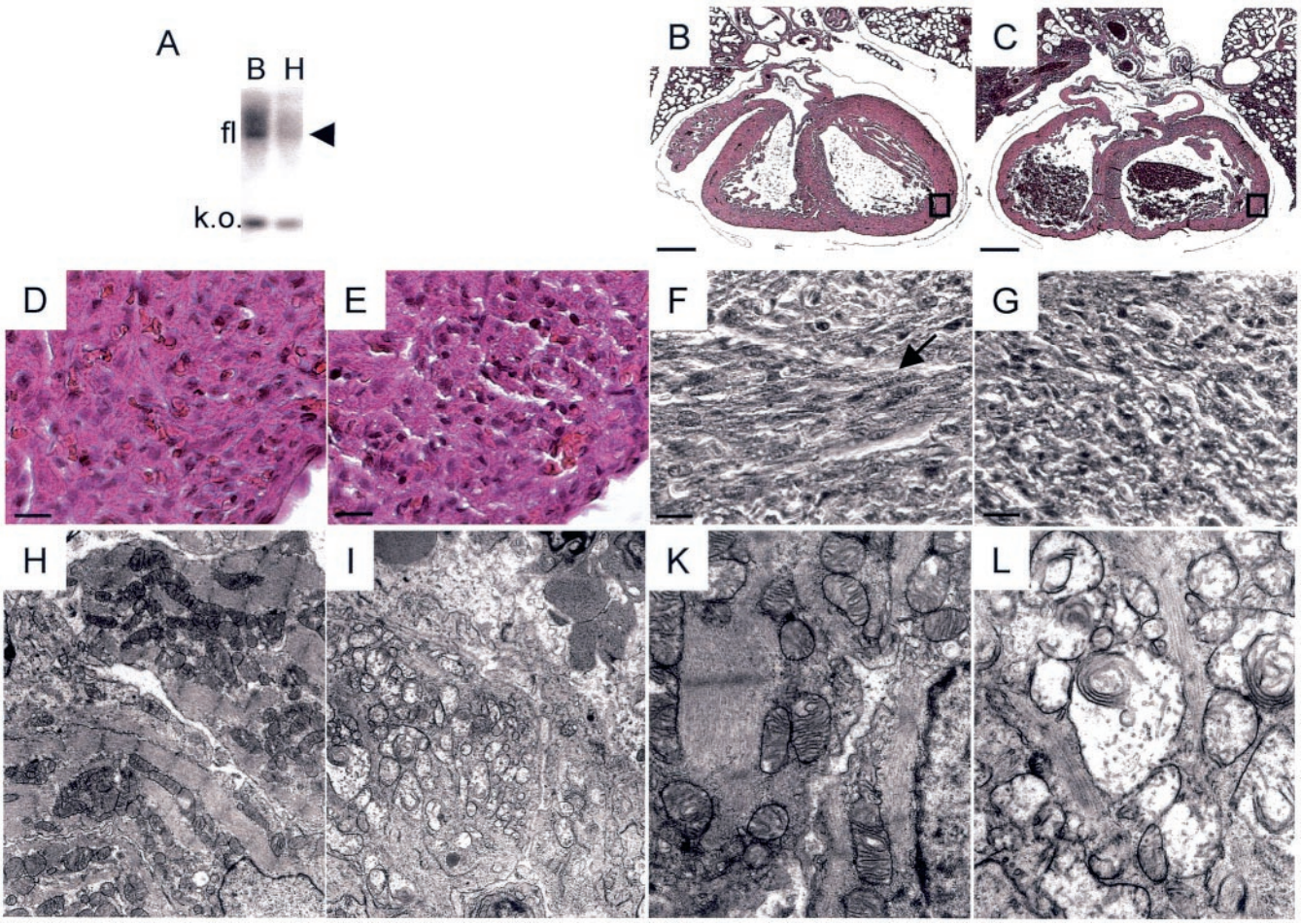

FIG. 5. Dilated congestive cardiomyopathy in heart-specific *TrxR2* KO mice. (A) Southern blot analysis revealed a decrease of the floxed allele (arrow) relative to the KO band in heart (lane H) compared to brain tissue (lane B). (B and C) Myocardial thinning and dilatation in cardiac tissue-specific $TrxR2^{-/-}$ mice (C). The ventricles and lung vessels were dilated and congested with blood cells. (D and E) Higher magnification of ventricular myocard (boxed in panels B and C) revealed nuclei of various sizes, massive vacuolization and perturbed directional arrangement of $TrxR2^{-/-}$ cardiomyocytes. (F and G) Phase-contrast imaging demonstrated strong reduction of cross-striation in KO cardiomyocytes (G) compared to control tissue (arrow in panel F). (H to L) Transmission electron microscopy revealed severe mitochondrial malformation and swelling with destruction or loss of cristae in KO myocardial (I and L) versus WT (H and K) cells at low (H and I) and high (K and L) magnifications. Scale bars: B and C, 250 μm; D to G, 10 μm.

step in GSH synthesis, only WT but not KO MEFs were able to survive and proliferate (Fig. 4H). To test whether increased levels of ROS in $TrxR2^{-/-}$ MEFs are responsible for the failure of cell survival when GSH synthesis is inhibited, we stained MEFs with the RedoxSensor Red CC-1 dye. In the presence of BSO, RedoxSensor Red CC-1 was predominantly localized in lysosomes of WT cells and in mitochondria of $TrxR2^{-/-}$ cells (Fig. 4I to L). Treatment of cells with the antioxidant *N*-acetylcysteine (NAC) rescued $TrxR2^{-/-}$ MEFs from BSO-induced apoptosis (Fig. 4H and M). These data indicate that under limiting GSH conditions TrxR2 is indispensable for sustaining cell survival in fibroblasts.

Heart-specific inactivation of TrxR2 leads to fatal dilated cardiomyopathy. Targeted disruption of genes such as *retinoid X receptor* α (5) and the cytokine receptor *gp130* (40) has suggested that these genes participate in heart and blood development. However, cardiomyocyte-specific inactivation of the respective genes did not support the conclusions drawn from the complete KO experiments (3, 10). To rule out the possibility that the failure in heart development is the consequence of a primary defect of *TrxR2* deficiency in hematopoietic cells, *TrxR2* was deleted specifically in cardiomyocytes by using the *MLC2a-Cre* transgenic mouse line (38). $TrxR2^{+/-}$ mice were first crossed with *MLC2a-Cre* mice and, subsequently, $TrxR2^{+/-,Tg[MLC2a\text{-}Cre]}$ and $TrxR2^{fl/fl}$ mice were mated to obtain $TrxR2^{fl/-,Tg[MLC2a\text{-}Cre]}$ mice. Mice that had both copies of the *TrxR2* gene deleted in a cardiac tissue-specific manner showed clinical features of congestive heart failure, including generalized edema, liver congestion, globular heart shape, and atrial dilatation, and died within several hours after birth (data not shown). Histological examination revealed dilated heart cavities and thinning of the ventricular myocardium (Fig. 5B and C). We observed, at higher magnifications, severe distortion in the morphology of myocardial cells, such as pycnotic nuclei, cytoplasmic vacuolization, and reduced cross-striation (Fig. 5D to G). Electron microscopic analyses of neonatal

hearts showed severe swelling and destruction of mitochondrial cristae in cardiomyocytes of cardiac tissue-restricted *TrxR2*-deficient mice (Fig. 5H to L). Vessel formation of yolk sac and placenta, as well as development of coronary arteries, as assessed by histological and immunohistochemical examination (vWF staining), was not affected by heart-specific inactivation of TrxR2 (data not shown). This demonstrates that TrxR2 is not only essential for normal embryonic hematopoiesis but also plays a crucial role in the maintenance of mitochondrial integrity in cardiomyocytes and is therefore indispensable for proper heart function of newborn mice.

DISCUSSION

Impairment or ablation of antioxidant enzymes leading to the accumulation of toxic levels of ROS might initiate or promote a variety of human diseases, e.g., neurodegeneration, cancer development, arthritis, and atherosclerosis. Many studies have addressed the role of GSH and GSH peroxidases as central regulators in the maintenance of the cellular redox balance. To assess the importance of the thioredoxin/thioredoxin reductase system in this process, we generated and analyzed mice with a nonfunctional TrxR2, a key enzyme of the mitochondrial redox system. At present, very little is known about the physiological role of TrxR2. TrxR2 belongs to the family of selenoproteins that are characterized by one or several catalytically indispensable SeCys residues (16). Since cotranslational SeCys incorporation at the UGA codon is very inefficient (35), overexpression studies are strongly limited in vitro and in vivo. For this reason, gene inactivation methods in mice offer a promising strategy.

Anticipating that loss of TrxR2 might be associated with embryonic death, we used the cre/loxP technology for the generation of *TrxR2* KO mice. Cre-mediated excision of the last four exons leads to the removal of the final 100 amino acids including the C terminally located redox-center consisting of Cys-SeCys-Gly. Mutational and biochemical studies have previously shown that SeCys is essential for the enzymatic function of TrxRs (9, 17, 41). Also, this approach deemed necessary because the 5′ region of *TrxR2* overlaps with the first exon of the *catechol-o-methyltransferase* gene, and there is also alternative first exon usage in the *TrxR2* gene (22, 34).

We found that during development *TrxR2* is mainly expressed in the embryonic heart and liver, reflecting the adult situation (22). This expression profile associates TrxR2 function with organs characterized by high metabolic activity and further corroborates a crucial role for TrxR2 in the control of harmful intracellular ROS.

Ubiquitous deletion of the *TrxR2* gene leads to embryonic lethality at E13. The phenotypic characteristics of $TrxR2^{-/-}$ embryos reflected the expression pattern of *TrxR2* in normal development. *TrxR2*-null embryos were highly anemic and smaller compared to WT littermates. Histological examination of the heart revealed that the ventricular walls and the trabeculae were thinner in KO mice than in WT and $TrxR2^{+/-}$ mice. The number of ISEL-positive cells was increased in the liver but not in the heart. In CFU assays established from fetal liver at E13, the size of all types of hematopoietic colonies was dramatically reduced, whereas hematopoietic differentiation was not affected by *TrxR2* deficiency.

Outgrowth of $TrxR2^{-/-}$ MEFs in tissue culture was also impaired but not to the same extent as observed for hematopoietic cells. $TrxR2^{-/-}$ fibroblasts could be propagated in vitro; they were, however, much more sensitive to oxidative stress imposed to the cells by GSH depletion than $TrxR2^{+/+}$ and $TrxR2^{+/-}$ cells. These data indicate that under standard cell culture conditions hematopoietic cells are more dependent on TrxR2 than fibroblasts. Several mechanisms, either alone or in combination, may account for the proposed hierarchy in TrxR2 dependence. Cells may differ in their ability to cope with oxygen radicals due to different degrees of pathway redundancy and/or overall antioxidant capacity. Alternatively, oxygen radical production of different cell types may vary greatly due to differences in their cellular metabolism. Finally, different cell types may differ widely in their intrinsic susceptibility versus resistance to oxygen radical-induced apoptosis due to different expression patterns of pro- and antiapoptotic proteins. The hematopoietic system is well known for its selective sensitivity to ionizing irradiation. Our finding that *TrxR2* KO mice die of anemia at day 13 of embryonic development may thus emphasize the particular susceptibility of hematopoietic cells to oxygen radical-induced apoptosis. This interpretation is in line with the fact that deletion of *Trx2* in the chicken B-cell line DT40 leads to oxygen-radical induced apoptosis mediated by cytochrome *c* release and caspase-3 activation (37).

The TrxR2 inactivation phenotype is less severe than the one observed in the KO mice of *Trx2*, the main substrate of TrxR2. $Trx2^{-/-}$ mice die at E10.5 due to massive apoptosis (26). This suggests that other enzymes, such as, for example, TrxR1 or the GSH-dependent redox system, can partially substitute for the *TrxR2* deficiency.

Besides the defect in hematopoiesis, *TrxR2* KO mice exhibited morphological changes in the heart. To discriminate whether TrxR2 plays an intrinsic role in heart development and function or whether the defect in heart morphology is a consequence of the defect in hematopoiesis, we bypassed the hematopoietic phenotype and established cardiac tissue-restricted *TrxR2*-deficient mice. These mice died shortly after birth from dilated cardiomyopathy and congestive heart failure. High-magnification and ultrastructural examination revealed severe distortion in the morphology of cardiomyocytes, i.e., pycnotic nuclei, partial loss of cross-striation, swelling of the mitochondria, and destruction of mitochondrial cristae. In contrast to the severe changes in morphology, no signs of apoptosis were detected in the myocardium by ISEL staining. Difficulties in detecting apoptotic cells in morphologically severely perturbed heart tissue have also been noted by others. Narula et al. found that cardiomyocytes of patients with idiopathic dilated or ischemic cardiomyopathy exhibit severe mitochondrial swelling and accumulation of cytochrome *c* in the cytosol in the absence of apoptotic changes (24). Likewise, the apoptotic index as defined by the TUNEL (terminal deoxynucleotidyltransferase-mediated dUTP-biotin nick end labeling) assay was found to be very low in models of chronic heart failure (12, 18). We suggest that cardiac tissue-restricted *TrxR2* KO mice die of congestive heart failure due to mitochondrial dysfunction of cardiomyocytes before DNA degradation and cell death of cardiomyocytes can be detected to a significant extent.

The fact that mice with cardiac tissue-specific deletion of

TrxR2 die shortly after birth has two implications. First, it indicates that the defect in heart morphology observed in *TrxR2*$^{-/-}$ mice at E13 is not only a consequence of the hematopoietic defect. It demonstrates for the first time that loss of one member of the Trx/TrxR system is indispensable for normal heart development and function. Second, lethality in complete *TrxR2*$^{-/-}$ embryos is delayed from E13 until birth in mice with a cardiac tissue-specific deletion of *TrxR2*. This suggests that the heart-specific defect observed in *TrxR2*$^{-/-}$ mice at E13 is not limiting on its own for survival during embryonic development. However, *TrxR2* deficiency in cardiomyocytes becomes fatal when an entirely self-sustaining circulatory system has to be maintained by the heart. It is conceivable that in mice with ubiquitous deletion of *TrxR2*, anemia and the heart-specific defect enhance each other and, thus, may lead to an earlier lethal compound phenotype compared to the respective tissue specific deletions. To clarify this issue, it would be necessary to generate a hematopoiesis-specific KO of *TrxR2*.

Using transgenic approaches, Yamamoto et al. demonstrated that *Trx1* is involved in cardiac myocyte growth of mice (39). Heart-specific overexpression of a dominant-negative form of Trx1 led to increased oxidative stress in cardiomyocytes associated with cardiac hypertrophy, whereas overexpression of WT *Trx1* reduced the extent of ROS-induced hypertrophy in response to pressure overload. Since the dominant-negative Trx1 may impair Trx2 activity as well, a putative contribution of Trx2 in protection of cardiomyocytes in this model seems likely. The perinatal lethality in our heart-specific *TrxR2* KO model precludes at present a detailed study of heart function parameters. Crossing the conditional *TrxR2* KO mice with the inducible heart-specific MERCreMER mice might generate a valuable tool for studying the impact of *TrxR2* deficiency on adult heart physiology (32).

A first indication that selenium is essential for heart function came from patients suffering from Keshan disease, a selenium deficiency disease endemic in China. Severely selenium-depleted humans show dilated congestive cardiomyopathy resembling the histopathologic phenotype of Friedreich's cardiomyopathy (28) and the phenotype observed in the *TrxR2*$^{-/-}$ mice. It is plausible that TrxR2 is the most likely candidate whose function is impaired in Keshan disease due to selenium deficiency. Whether functional impairment of other selenoproteins also contributes to the pathophysiology of this disease remains an open question. It is also noteworthy that *TrxR2* is localized to chromosome *22q11*, a region deleted in the human haploinsufficiency velo-cardio-facial/DiGeorge Syndrome (VCS/DGS) (13, 19, 20). Hallmarks of VCS/DGS have not been noticed in hemizygous/homozygous or in cardiac tissue-restricted *TrxR2* KO mice (data not shown). Further studies will address the question whether loss of one *TrxR2* allele may contribute to the compound VCS/DGS phenotype.

ACKNOWLEDGMENTS

We are grateful to C. Neumüller and J. Plitzko for help with the heart ultrastructure analysis, A. Geishauser and M. Semisch for excellent technical work, and the personnel of the animal facility and blastocyst injection unit at GSF for excellent assistance and support.

This study was supported by the DFG-Priority Programme SPP1087, by Fonds der Chemischen Industrie, and a fellowship from the Humboldt-Stiftung to S.G.M.; by the DFG Priority Programme 1069 "Angiogenesis" (HA 2983/1-2) and the German Human Genome Project (DHGP 9907) to A.K.H.; and by the BMBF to W.W.

REFERENCES

1. **Arner, E. S., and A. Holmgren.** 2000. Physiological functions of thioredoxin and thioredoxin reductase. Eur. J. Biochem. **267:**6102–6109.
2. **Chen, C. S., and K. R. Gee.** 2000. Redox-dependent trafficking of 2,3,4,5,6-pentafluorodihydrotetramethylrosamine, a novel fluorogenic indicator of cellular oxidative activity. Free Radic. Biol. Med. **28:**1266–1278.
3. **Chen, J., S. W. Kubalak, and K. R. Chien.** 1998. Ventricular muscle-restricted targeting of the RXRα gene reveals a non-cell-autonomous requirement in cardiac chamber morphogenesis. Development **125:**1943–1949.
4. **Conrad, M., M. Brielmeier, W. Wurst, and G. W. Bornkamm.** 2003. Optimized vector for conditional gene targeting in mouse embryonic stem cells. BioTechniques **34:**1136–1140.
5. **Dyson, E., H. M. Sucov, S. W. Kubalak, G. W. Schmid-Schonbein, F. A. DeLano, R. M. Evans, J. Ross, Jr., and K. R. Chien.** 1995. Atrial-like phenotype is associated with embryonic ventricular failure in retinoid X receptor alpha$^{-/-}$ mice. Proc. Natl. Acad. Sci. USA **92:**7386–7390.
6. **Dzierzak, E., and A. Medvinsky.** 1995. Mouse embryonic hematopoiesis. Trends Genet. **11:**359–366.
7. **Gasdaska, P. Y., M. M. Berggren, M. J. Berry, and G. Powis.** 1999. Cloning, sequencing and functional expression of a novel human thioredoxin reductase. FEBS Lett. **442:**105–111.
8. **Gasdaska, P. Y., J. R. Gasdaska, S. Cochran, and G. Powis.** 1995. Cloning and sequencing of a human thioredoxin reductase. FEBS Lett. **373:**5–9.
9. **Gorlatov, S. N., and T. C. Stadtman.** 1998. Human thioredoxin reductase from HeLa cells: selective alkylation of selenocysteine in the protein inhibits enzyme activity and reduction with NADPH influences affinity to heparin. Proc. Natl. Acad. Sci. USA **95:**8520–8525.
10. **Hirota, H., J. Chen, U. A. Betz, K. Rajewsky, Y. Gu, J. Ross, Jr., W. Muller, and K. R. Chien.** 1999. Loss of a gp130 cardiac muscle cell survival pathway is a critical event in the onset of heart failure during biomechanical stress. Cell **97:**189–198.
11. **Hogan, B., R. Beddington, F. Costantini, and E. Lacy.** 1994. Manipulating the mouse embryo: a laboratory manual, 2nd ed. Cold Spring Harbor Laboratory Press, Cold Spring Harbor, N.Y.
12. **Hughes, S. E.** 2003. Detection of apoptosis using in situ markers for DNA strand breaks in the failing human heart: fact or epiphenomenon? J. Pathol. **201:**181–186.
13. **Jerome, L. A., and V. E. Papaioannou.** 2001. DiGeorge syndrome phenotype in mice mutant for the T-box gene, Tbx1. Nat. Genet. **27:**286–291.
14. **Joyner, A. L.** 2000. Gene targeting: a practical approach, 2nd ed. Oxford University Press, New York, N.Y.
15. **Kim, M. R., H. S. Chang, B. H. Kim, S. Kim, S. H. Baek, J. H. Kim, S. R. Lee, and J. R. Kim.** 2003. Involvements of mitochondrial thioredoxin reductase (TrxR2) in cell proliferation. Biochem. Biophys. Res. Commun. **304:**119–124.
16. **Kryukov, G. V., S. Castellano, S. V. Novoselov, A. V. Lobanov, O. Zehtab, R. Guigo, and V. N. Gladyshev.** 2003. Characterization of mammalian selenoproteomes. Science **300:**1439–1443.
17. **Lee, S. R., S. Bar-Noy, J. Kwon, R. L. Levine, T. C. Stadtman, and S. G. Rhee.** 2000. Mammalian thioredoxin reductase: oxidation of the C-terminal cysteine/selenocysteine active site forms a thioselenide, and replacement of selenium with sulfur markedly reduces catalytic activity. Proc. Natl. Acad. Sci. USA **97:**2521–2526.
18. **Li, Z., O. H. Bing, X. Long, K. G. Robinson, and E. G. Lakatta.** 1997. Increased cardiomyocyte apoptosis during the transition to heart failure in the spontaneously hypertensive rat. Am. J. Physiol. **272:**H2313–H2319.
19. **Lindsay, E. A., F. Vitelli, H. Su, M. Morishima, T. Huynh, T. Pramparo, V. Jurecic, G. Ogunrinu, H. F. Sutherland, P. J. Scambler, A. Bradley, and A. Baldini.** 2001. Tbx1 haploinsufficiency in the DiGeorge syndrome region causes aortic arch defects in mice. Nature **410:**97–101.
20. **Merscher, S., B. Funke, J. A. Epstein, J. Heyer, A. Puech, M. M. Lu, R. J. Xavier, M. B. Demay, R. G. Russell, S. Factor, K. Tokooya, B. S. Jore, M. Lopez, R. K. Pandita, M. Lia, D. Carrion, H. Xu, H. Schorle, J. B. Kobler, P. Scambler, A. Wynshaw-Boris, A. I. Skoultchi, B. E. Morrow, and R. Kucherlapati.** 2001. TBX1 is responsible for cardiovascular defects in velo-cardio-facial/DiGeorge syndrome. Cell **104:**619–629.
21. **Miranda-Vizuete, A., A. E. Damdimopoulos, and G. Spyrou.** 1999. cDNA cloning, expression, and chromosomal localization of the mouse mitochondrial thioredoxin reductase gene. Biochim. Biophys. Acta **1447:**113–118.
22. **Miranda-Vizuete, A., and G. Spyrou.** 2002. Genomic organization and identification of a novel alternative splicing variant of mouse mitochondrial thioredoxin reductase (TrxR2) gene. Mol. Cells **13:**488–492.
23. **Mustacich, D., and G. Powis.** 2000. Thioredoxin reductase. Biochem. J. **346**(Pt. 1)**:**1–8.
24. **Narula, J., P. Pandey, E. Arbustini, N. Haider, N. Narula, F. D. Kolodgie, B. Dal Bello, M. J. Semigran, A. Bielsa-Masdeu, G. W. Dec, S. Israels, M. Ballester, R. Virmani, S. Saxena, and S. Kharbanda.** 1999. Apoptosis in heart failure: release of cytochrome c from mitochondria and activation of

caspase-3 in human cardiomyopathy. Proc. Natl. Acad. Sci. USA **96:**8144–8149.

25. **Neumann, C. A., D. S. Krause, C. V. Carman, S. Das, D. P. Dubey, J. L. Abraham, R. T. Bronson, Y. Fujiwara, S. H. Orkin, and R. A. Van Etten.** 2003. Essential role for the peroxiredoxin Prdx1 in erythrocyte antioxidant defense and tumour suppression. Nature **424:**561–565.
26. **Nonn, L., R. R. Williams, R. P. Erickson, and G. Powis.** 2003. The absence of mitochondrial thioredoxin 2 causes massive apoptosis, exencephaly, and early embryonic lethality in homozygous mice. Mol. Cell. Biol. **23:**916–922.
27. **Nordberg, J., and E. S. Arner.** 2001. Reactive oxygen species, antioxidants, and the mammalian thioredoxin system. Free Radic. Biol. Med. **31:**1287–1312.
28. **Puccio, H., D. Simon, M. Cossee, P. Criqui-Filipe, F. Tiziano, J. Melki, C. Hindelang, R. Matyas, P. Rustin, and M. Koenig.** 2001. Mouse models for Friedreich ataxia exhibit cardiomyopathy, sensory nerve defect and Fe-S enzyme deficiency followed by intramitochondrial iron deposits. Nat. Genet. **27:**181–186.
29. **Schaft, J., R. Ashery-Padan, F. van der Hoeven, P. Gruss, and A. F. Stewart.** 2001. Efficient FLP recombination in mouse ES cells and oocytes. Genesis **31:**6–10.
30. **Schroeder, T., S. T. Fraser, M. Ogawa, S. Nishikawa, C. Oka, G. W. Bornkamm, T. Honjo, and U. Just.** 2003. Recombination signal sequence-binding protein Jκ alters mesodermal cell fate decisions by suppressing cardiomyogenesis. Proc. Natl. Acad. Sci. USA **100:**4018–4023.
31. **Schwenk, F., U. Baron, and K. Rajewsky.** 1995. A cre-transgenic mouse strain for the ubiquitous deletion of loxP-flanked gene segments including deletion in germ cells. Nucleic Acids Res. **23:**5080–5081.
32. **Sohal, D. S., M. Nghiem, M. A. Crackower, S. A. Witt, T. R. Kimball, K. M. Tymitz, J. M. Penninger, and J. D. Molkentin.** 2001. Temporally regulated and tissue-specific gene manipulations in the adult and embryonic heart using a tamoxifen-inducible Cre protein. Circ. Res. **89:**20–25.
33. **Sun, Q. A., L. Kirnarsky, S. Sherman, and V. N. Gladyshev.** 2001. Selenoprotein oxidoreductase with specificity for thioredoxin and glutathione systems. Proc. Natl. Acad. Sci. USA **98:**3673–3678.
34. **Sun, Q. A., F. Zappacosta, V. M. Factor, P. J. Wirth, D. L. Hatfield, and V. N. Gladyshev.** 2001. Heterogeneity within animal thioredoxin reductases: evidence for alternative first exon splicing. J. Biol. Chem. **276:**3106–3114.
35. **Suppmann, S., B. C. Persson, and A. Bock.** 1999. Dynamics and efficiency in vivo of UGA-directed selenocysteine insertion at the ribosome. EMBO J. **18:**2284–2293.
36. **Tanaka, H., I. Matsumura, S. Ezoe, Y. Satoh, T. Sakamaki, C. Albanese, T. Machii, R. G. Pestell, and Y. Kanakura.** 2002. E2F1 and c-Myc potentiate apoptosis through inhibition of NF-κB activity that facilitates MnSOD-mediated ROS elimination. Mol. Cell **9:**1017–1029.
37. **Tanaka, T., F. Hosoi, Y. Yamaguchi-Iwai, H. Nakamura, H. Masutani, S. Ueda, A. Nishiyama, S. Takeda, H. Wada, G. Spyrou, and J. Yodoi.** 2002. Thioredoxin-2 (TRX-2) is an essential gene regulating mitochondrion-dependent apoptosis. EMBO J. **21:**1695–1703.
38. **Wettschureck, N., H. Rutten, A. Zywietz, D. Gehring, T. M. Wilkie, J. Chen, K. R. Chien, and S. Offermanns.** 2001. Absence of pressure overload induced myocardial hypertrophy after conditional inactivation of Gαq/Gα11 in cardiomyocytes. Nat. Med. **7:**1236–1240.
39. **Yamamoto, M., G. Yang, C. Hong, J. Liu, E. Holle, X. Yu, T. Wagner, S. F. Vatner, and J. Sadoshima.** 2003. Inhibition of endogenous thioredoxin in the heart increases oxidative stress and cardiac hypertrophy. J. Clin. Investig. **112:**1395–1406**.**
40. **Yoshida, K., T. Taga, M. Saito, S. Suematsu, A. Kumanogoh, T. Tanaka, H. Fujiwara, M. Hirata, T. Yamagami, T. Nakahata, T. Hirabayashi, Y. Yoneda, K. Tanaka, W. Z. Wang, C. Mori, K. Shiota, N. Yoshida, and T. Kishimoto.** 1996. Targeted disruption of gp130, a common signal transducer for the interleukin 6 family of cytokines, leads to myocardial and hematological disorders. Proc. Natl. Acad. Sci. USA **93:**407–411.
41. **Zhong, L., and A. Holmgren.** 2000. Essential role of selenium in the catalytic activities of mammalian thioredoxin reductase revealed by characterization of recombinant enzymes with selenocysteine mutations. J. Biol. Chem. **275:**18121–18128.